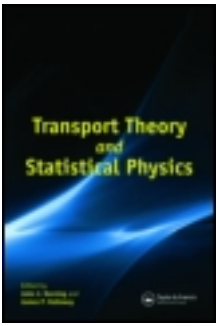

Transport Theory and Statistical Physics

Publication details, including instructions for authors and subscription information:
http://www.tandfonline.com/loi/ltty20

p-adaptive numerical methods for particle transport

James S. Warsa [a] & Anil K. Prinja [a]

[a] University of New Mexico, Department of Chemical and Nuclear Engineering, Albuquerque, NM, 87131

Version of record first published: 20 Aug 2006.

To cite this article: James S. Warsa & Anil K. Prinja (1999): p-adaptive numerical methods for particle transport, Transport Theory and Statistical Physics, 28:3, 229-270

To link to this article: http://dx.doi.org/10.1080/00411459908206036

TRANSPORT THEORY AND STATISTICAL PHYSICS, 28(3), 229–270 (1999)

p-ADAPTIVE NUMERICAL METHODS FOR PARTICLE TRANSPORT

James S. Warsa and Anil K. Prinja

University of New Mexico
Department of Chemical and Nuclear Engineering
Albuquerque, NM 87131

ABSTRACT

A p-adaptive method is applied to the discrete ordinates form of the monoenergetic transport equation in one dimension. Discontinuous spatial discretizations of arbitrary accuracy are generated in a finite element context using the computer algebra program MAPLE. Source code for the high order methods is produced automatically by MAPLE and then implemented in a discrete ordinates neutral particle transport code in an adaptive fashion. The degree, p, of the polynomial representation used on a mesh cell is varied during the course of the source iterations and the corresponding order of accuracy increased or decreased according to some selected tolerance specification. The accuracy and other numerical properties of the method are investigated and the results of numerical computations are presented.

1. INTRODUCTION

In this paper we discuss an adaptive method for numerically solving the discrete ordinates form of the steady-state neutral particle transport equation in one spatial dimension.

The study of numerical methods for solving the transport equation has long been an area of active research. The potential of a given algorithm is

usually measured by its computational complexity relative to other methods of similar accuracy. The question of positivity, that is, whether or not the numerical solution is positive provided that the source term and other transport parameters are positive, is another (largely "psychological"[1]) concern. Other properties, such as linearity, numerical conservation, a consistent diffusion limit, flux continuity,[2] stability, and amenability to acceleration techniques, are also often considered.

The three factors considered most desirable, accuracy, simplicity and positivity, interact with one another in a game of give-and-take;[3] improving or focusing on one of these aspects is often at the expense of another. For instance, making a method positive might make it more complicated or less accurate or, possibly, both. Alternately, keeping a method simple might require that it is not accurate. Similarly, achieving high accuracy might require a scheme that is inefficient or not positive. However, it is also true that a more accurate solution is more likely to be positive since real, physical solutions are positive. Different numerical methods preserve these properties to varying degrees and have differing effects on other numerical characteristics as well. Many approaches have been developed over the past several decades, including some schemes that are quite convoluted and/or non-linear, to synthesize as many desirable properties as possible in a single method.

With today's available computing power, simplicity is no longer the principal factor it once was, although it could be argued that in multiple dimensions it cannot be ignored completely. Non-linear negative flux fixup schemes designed to restore positivity can also destroy the simplicity of the original algorithms and might also degrade their accuracy. The new exponential discontinuous scheme, for example, although strictly positive requires an iterative root find for the exponential constant on each mesh cell[4,5] adding greatly to the computational expense of the method.

The importance of positivity is a highly subjective value and one that might be ignored by the numerical analyst, though perhaps not by someone who is interested in developing a production reactor physics code, for example, and does not wish to produce negative fluxes or reaction rates under a wide variety of circumstances. Another situation in which positive

fluxes are desired is when the results of a computation are to be used as a source for further transport calculations. It has also been pointed out[1,6–8] that negative fluxes, or negative-flux fix-ups, can interfere with other aspects of a solution method leading to instabilities. Of course, in reality the angular flux is non-negative and one cannot ascribe physical meaning to negative particle distributions. For reasons such as this, a great deal of effort is concentrated on trying to make non-positive methods positive[9,10] while retaining accuracy.

Much work has been done to investigate and improve the accuracy of various numerical methods since the 1940s through the present day. This vast collection of work includes a wide range of discretizations, methods, regimes, implementations, and applications, many of which are highly specialized, sometimes sophisticated, and often focused on particular aspects of a certain problem or solution.

In this paper, we will consider the spatial discretization of the discrete ordinates, or S_N, method. The nodal formalism first put forth by Hennart[11] and later extended and generalized by Hennart and del Valle[12–14] is an attempt to systematically unify the various finite difference, nodal, characteristic and finite element methods, with both continuous and discontinuous spatial discretizations. Recent non-linear schemes[4,5,15] are not encompassed by that investigation. Hennart's formalism carries over directly to the analysis of finite element methods, which have been widely used in the numerical solution of the transport equation,[16–24] and which forms the basis of our work. We note also that Azmy[25] has developed nodal methods of general order accuracy for two-dimensional transport in weighted diamond-difference form.

The Galerkin procedure used in the development of finite element methods generates, in a direct and mechanical way, discrete weak form solutions that have an arbitrarily high order of accuracy. We have derived spatially discretized numerical solution methods using the symbolic algebra program MAPLE[26] to carry out the mathematical manipulations of the Galerkin procedure of the finite element formalism. The resulting high order methods are used to to compute solutions in an adaptive way on fixed meshes. This is not a totally new idea, as so-called *p*-adaptive methods have often been

used in the area computational fluid dynamics,[27,28] structural analysis,[29,30] and recently in diffusion analysis for reactor physics.[31] In such an approach, the degree p of the interpolating polynomial on the discretized domain is varied during the course of the computation. This is done dynamically and automatically, using a high degree in some regions of the problem and a low degree in others, dictated by the solution itself. Increasing the degree of the polynomial increases the order of accuracy and it is expected that the accuracy of the solution will be improved. By this we mean that a more accurate solution will be locally achieved. This may not necessarily lead to a global improvement in accuracy. However, a more accurate solution, which is therefore more likely to be positive in localized areas of the domain where the numerical solution might otherwise become negative, does have the potential to improve the overall positivity by preventing the propagation of negative fluxes.

Our approach is based on the linear (LD) and bi-linear discontinuous (BLD) methods used, respectively, in one and two dimensional transport applications.[22–24,32] A novel aspect of this work is the use of MAPLE to extend the LD methods to polynomial representations of arbitrary degree in such a way as to automatically generate Fortran or C code fragments that can then be included in a transport code.

The foremost question, then, is whether the increased computational demands associated with the adaptive scheme are outweighed by improved accuracy or other desirable numerical properties. Though it might not be true in one dimension, further work could show it is true for certain energy dependent problems or in higher dimensions whose solutions can exhibit (nearly) discontinuous solutions.

It is easy to envision applications for which the p-adaptive method (or extensions of it to other domains) could be very useful. One application might be for problems with a mesh grid that cannot be easily refined, for example one whose geometry is specified by a complicated three-dimensional CAD model. Another could be for problems whose input data is for whatever reason fixed at a certain level of discretization, for instance an energy dependent cross section set that is determined empirically or that is not easily recalculated on another grid. Should higher accuracy be required in

such situations, it might be easier and more efficient to allow the computer program to determine the required level of approximation and corresponding order of accuracy, automatically and only where necessary, than it would be to recompute the input data and solution on a refined grid.

This paper is organized as follows. The next section introduces the finite element formalism for the spatial discretization and the MAPLE implementation. The third section gives a brief account of some of the numerical properties of the high order methods so generated. In Section 4, the *p*-adaptive implementation is discussed. In the fifth section, numerical results are presented and compared. The last section concludes the paper with some summary remarks and indications for future work.

2. GENERATING HIGH ORDER METHODS

In this section we present a formalism for generating high order accurate numerical methods in the spatial variable x for the monoenergetic transport equation in plane geometry:

$$\mu\frac{\partial\psi(x,\mu)}{\partial x}+\sigma_t(x)\psi(x,\mu)=\int_0^{2\pi}d\phi'\int_{-1}^{1}d\mu'\sigma_s(x,\mu_0)\psi(x,\mu')+Q(x,\mu). \tag{1}$$

This is in standard notation. We want to solve this equation for the angular flux $\psi(x,\mu)$. Here $Q(x,\mu)$ represents an external source of particles, $\sigma_t(x)$ and $\sigma_s(x)$ represent the total and scattering interaction probabilities, respectively, and the lab system scattering angle cosine is

$$\mu_0=\mu'\mu+\left[(1-\mu'^2)(1-\mu^2)\right]^{1/2}\cos(\phi'). \tag{2}$$

We consider the discrete ordinates equations

$$\mu_m\frac{d\psi_m^k(x)}{dx}+\sigma_t(x)\psi_m^k(x)=\sum_{l=0}^{L}\frac{2l+1}{2}\sigma_l(x)P_l(\mu_m)\phi_l(x)+Q_m(x),\quad m=1\ldots M. \tag{3}$$

A quadrature set of nodes and weights $\{\mu_m,w_m\}_{m=1}^{M}$, on the angular domain $\mu\epsilon[-1,1]$ with

$$\sum_{m=1}^{M} w_m = 2.0, \tag{4}$$

collocates the angular flux at the discrete nodes of the quadrature such that $\psi_m(x) \approx \psi(x, \mu_m)$. The quadrature is used to compute the scalar flux moments

$$\phi_l(x) \approx \sum_{m=1}^{M} w_m P_l(\mu_m)\psi_m(x). \tag{5}$$

We have allowed that the scattering kernel $\sigma_s(x, \mu_0)$ in Eq. 1 be anisotropic, and we have assumed that the scattering cross section has been expanded in a truncated series of Legendre polynomials

$$\sigma_s(x, \mu_0) = \sum_{l=0}^{L} \frac{2l+1}{4\pi}\sigma_l(x)P_l(\mu_0) \tag{6a}$$

and that the expansion coefficients $\sigma_l(x)$, defined by

$$\sigma_l(x) = 2\pi \int_{-1}^{1} d\mu_0 P_l(\mu_0)\sigma_s(x, \mu_0), \tag{6b}$$

are given.

In order to more accurately model a normally incident beam, we use a Lobatto quadrature which has nodes fixed at $\mu = \pm 1$. On one face of the slab, the left side at $x = 0$, for example, we set

$$\psi_m(0) = \begin{cases} w_m^{-1} & \text{for } m \text{ where } \mu_m = 1, \\ 0 & \text{otherwise,} \end{cases} \tag{7a}$$

or, for an isotropic source, we set

$$\psi_m(0) = 2 \quad \text{for all } m. \tag{7b}$$

These boundary conditions are typically normalized to give a unit incident current.

On the other face of the slab we will consider either a vacuum boundary condition, that is zero flux for the incoming directions at $x = a$:

$$\psi_m(a) = 0 \quad \text{for all } m \text{ such that } \mu_m < 0, \tag{7c}$$

or a reflective condition where the incoming fluxes at $x = a$ are equal to the outgoing fluxes for symmetric angular ordinates:

$$\psi_m(a) = \psi_{m'}(a) \quad \text{for } m \text{ such that } \mu_m > 0 \text{ and } \mu_m = -\mu_{m'}. \tag{7d}$$

For ease of exposition, we write the discrete ordinates equations in compact operator notation

$$\hat{H}_m \psi_m^k(x) = \hat{S}\psi_m^{k-1} + Q_m(x), \quad m = 1 \ldots M, \tag{8}$$

where the definitions of the operators follow from Eq. 3.

2.1. Spatial Discretization

We now consider the discretization of the spatial variable x in the transport equation.

The spatial domain $x \in [0, a]$ is divided into a mesh of N_x intervals. The i^{th} interval is the mesh cell $x \in [x_{i-\frac{1}{2}}, x_{i+\frac{1}{2}}]$ and Δx_i is the width of the cell. The cross sections are piecewise constant on this interval such that $\sigma_s(x) = \sigma_{si}$ and $\sigma_t(x) = \sigma_{ti}$.

Omitting for the time being the angle, mesh cell, and iteration indices, we approximate the solution of the transport equation, $\psi(x)$, as a polynomial of degree p for the cell i:

$$\psi(x) \approx \tilde{\psi}(x) = \sum_{n=0}^{p} \psi_n L_n(x). \tag{9}$$

The functions $L_n(x)$, the Lagrange polynomials for the $p+1$ equally spaced knots of the cell

$$x_n = x_{i-\frac{1}{2}} + \left[\frac{\Delta x_i}{p}\right], \quad n = 0 \ldots p,$$

are given by

$$L_n = \prod_{\substack{s=0 \\ s \neq n}}^{p} \frac{(x - x_s)}{(x_n - x_s)}, \quad n = 0 \ldots p. \tag{10}$$

A hypothetical polynomial approximation to the angular flux is illustrated in Figure 1. The approximate flux takes on the values of the coefficients in the Lagrange representation because these polynomials have the convenient property

$$L_n(x_s) = \delta_{ns} = \begin{cases} 0 & \text{for } s \neq n, \\ 1 & \text{for } s = n. \end{cases} \tag{11}$$

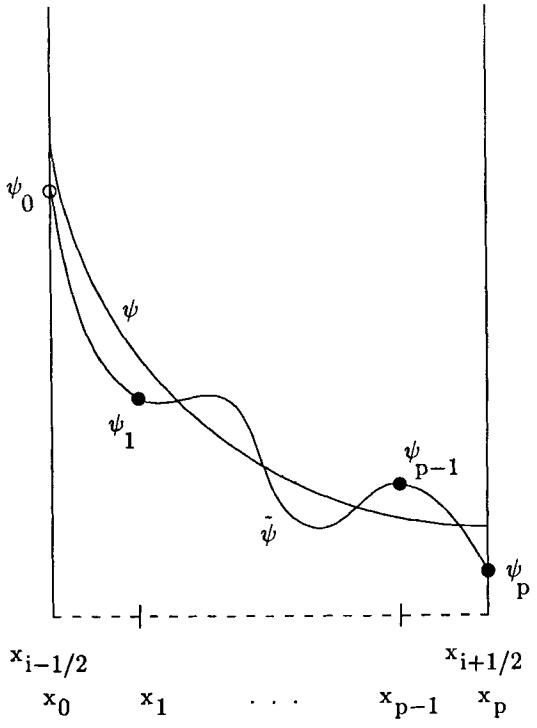

Figure 1

Spatial mesh cell i. The nodes of the spatial mesh are $x_{i+\frac{1}{2}}$ and $x_{i-\frac{1}{2}}$. The knots $x_0, \ldots, x_p$, of the $p+1$ Langrange basis functions are also shown.

where δ_{ns} is the Kronecker delta function. Note the leftmost circle representing the point ψ_0 is open indicating a discontinuity in the flux (for the case $\mu > 0$).

With this definition for the approximate angular flux we use the Galerkin method[16,17,20,21] to derive a high-order discretization scheme in the spatial variable x, keeping Figure 1 in mind.

The Galerkin procedure entails taking the inner products of the the residual of the transport equation with each of the basis functions and equating them to zero. This amounts to inserting the approximate flux expansion, Eq. 9, into the transport equation, Eq. 8, multiplying by each of the $p+1$

Lagrange basis functions, and integrating over the cell. Interchanging orders of summation and integration for the scattering term, we get the following $(p+1) \times (p+1)$ system of equations for a cell i:

$$\mu \int dx\, L_n(x) \frac{d\tilde{\psi}}{dx} + \sigma_t \int dx\, L_n(x) \tilde{\psi}(x) = \hat{S} \int dx\, L_n(x) \tilde{\psi}(x) + \int dx\, L_n(x) Q(x), \quad n = 0 \ldots p, \quad (12)$$

where the integrations are over $x \in [x_{i-\frac{1}{2}}, x_{i+\frac{1}{2}}]$ or, equivalently, $x \in [x_0, x_p]$.

The system of equations for the angular flux coefficients must be coupled to those of the neighboring cells. Either they are coupled because the form of the basis functions is such that they extend over one or more nearby cells, or the coupling takes place explicitly. The Lagrange form we use for the interpolating polynomial approximation on a cell means we must couple them explicitly.

An S_N iteration consists of a march back and forth across the spatial mesh once for each angle. The most recently computed angular fluxes are used to calculate the scattering source for the next iteration. With this marching scheme in mind, the mesh cells are coupled depending on the direction of particle flow.

It turns out that a method of greater accuracy is developed by allowing for discontinuities in the solution at the cell edges.[1,13,33–35] This requires two steps. First the term containing the derivative of the flux is integrated by parts (an application of Gauss' or Green's theorem in higher dimensions)

$$\mu \left[L_n(x) \tilde{\psi}(x) \right]_{x_0}^{x_p} - \mu \int_{x_0}^{x_p} dx\, \frac{dL_n(x)}{dx} \tilde{\psi}(x). \quad (13)$$

With the property Eq. 11 of the Lagrange basis functions the "boundary term", the first term in Eq. 13, only survives for the equations $n = 0$ and $n = p$. They are $-\mu\tilde{\psi}(x_0)$ and $\mu\tilde{\psi}(x_p)$, respectively.

Now we have a choice as to how we might couple the cells. For instance, to impose continuity in the flux at the cell boundary we would set the above fluxes to their values at the cell edges, $\tilde{\psi}(x_0) \to \psi_0$ and $\tilde{\psi}(x_p) \to \psi_p$. The system of equations could then be solved for the coefficients $\{\psi_n\}_{n=0}^{p}$ as they stand. In a computer implementation, the flux coefficient ψ_0 for the cell i would be set to the value of the outgoing flux ψ_p from the cell $i-1$

for $\mu > 0$, and, for $\mu < 0$, the value of ψ_p for cell i would be set to the value of ψ_0 from cell $i+1$. Note that we get the same result if we do not first perform the integration by parts and then solve the equations.

A discontinuity in the flux can be introduced, however, by setting $\tilde{\psi}(x_0)$ to ψ_p of the previous cell, cell $i-1$ for $\mu > 0$, and for $\mu < 0$ setting $\tilde{\psi}(x_p)$ to ψ_0 of the previous cell, cell $i+1$, before solving the system of equations.

The rest of the integrations in Eq. 12 can be carried out, including the remaining terms from the integration by parts. We assume a piecewise constant inhomogeneous source term, so that in the cell of interest $Q(x) = Q_i$ which can be brought outside the integral. The scattering terms for the S_N source iterations are generated by applying the scattering operator to each of the following inner products arising from application of the Galerkin method (the integrations being taken over a cell):

$$s_k = \int dx\, L_k(x)\tilde{\psi}(x) = \sum_{n=0}^{p} \psi_n \int dx\, L_n(x)L_k(x), \quad k = 0 \ldots p. \tag{14}$$

The source moments $\{\hat{S}s_n\}_{n=0}^{p}$ are computed at every iteration.

The system of equations, Eq. 12, was solved for the flux coefficients of various orders of p using the symbolic algebra computer program MAPLE[26] as were the corresponding source terms in Eq. 14. MAPLE was then used to generate optimized source code containing explicit Fortran expressions for the flux coefficients and source moments to be incorporated in a transport code. Computations were performed in 25 digits of software precision, and the Fortran files were written with about 15 digits of precision.

The algebraic manipulations required to solve the system of equations even for $p = 5$ or $p = 6$ are formidable, and a symbolic solution becomes tractable only with the MAPLE symbolic algebra program. Furthermore, once the lower order systems have been verified the expressions can be generated *without mistakes*. Running times ranged from about 4 cpu seconds for $p = 1$ to around 150 cpu minutes for the $p = 6$ case on an IBM RS6000 model 370 workstation. Of course, the system of equations can be solved numerically during the execution of the transport code. This may be done at different levels. The integrals in the Galerkin procedure can be computed symbolically and a matrix equation for the cell fluxes can be inverted numerically at each step of the spatial S_N march. This has been shown to be

much less efficient, up to 60% slower for the BLD method in Ref. [24], than evaluating explicit expressions for the cell fluxes. At the next level, even the integrals themselves may be evaluated numerically, as would be the case, perhaps, for complicated geometrical discretizations.

2.2. Accuracy, Positivity, and Stability

We use Hennart and del Valle's analysis[12–14] to show the order of accuracy of the high order methods described in the previous section. First we show that their formalism carries over directly to ours in order that we might quote their results.

They define the representation $\psi_h(x)$ of the flux on a cell in terms of shifted Legendre polynomials $p_j(x), j = 0 \ldots p$, orthogonal on $x \in [x_l, x_r]$ ($x_l = x_0$ and $x_r = x_p$), with appropriate normalization constants N_j on the cell. They write

$$\psi_h(x) = \psi_r p_k(x) + \sum_{j=0}^{k-1} \psi_c^j u_c^i(x), \tag{15a}$$

where

$$u_c^j(x) = p_j(x) - p_k(x), \quad j = 0 \ldots k-1. \tag{15b}$$

We must take the maximum degree of the Legendre polynomials to be $k = p$. The spatial cell moments of the flux are then defined as

$$\psi_c^j = m_c^j(\psi_h(x)) = \frac{1}{N_i} \int_{x_l}^{x_r} p_j(x) \psi_h(x) dx, \quad j = 0 \ldots k. \tag{16}$$

If we expand our basis functions $L_n(x)$ in terms of these polynomials as

$$L_n(x) = \sum_{j=0}^{k} b_{nj} p_j(x) \tag{17a}$$

where the b_{nj} are expansion coefficients given by

$$b_{nj} = \frac{1}{N_j} \int_{x_l}^{x_r} p_j(x) L_n(x) dx, \tag{17b}$$

then we can show that our approximation on the cell $\tilde{\psi}(x)$ can be written in terms of the Legendre polynomials as

$$\tilde{\psi}(x) = \sum_{j=0}^{k} \psi_c^j p_j(x) \tag{18a}$$

where

$$\psi_c^j = \sum_{n=0}^{k} b_{nj} \psi_n, \quad j = 0 \ldots k-1, \tag{18b}$$

and

$$\psi_c^k = \psi_r - \sum_{j=0}^{k-1} \psi_c^j. \tag{18c}$$

The ψ_n here are the expansion coefficients in Eq. 9. This establishes the equivalence between the two representations.

Having made this connection, we can use the results of the convergence proofs for the discontinuous case in Ref. [13] directly. It was shown that at the outgoing cell edge the truncation error is of order $2p+1$, and that the cell spatial moments, ψ_c^j, have an error of order $2p+1-j, j \leq p$. (note that $m_c^j(\psi_h(x)) = m_c^j(\tilde{\psi}(x))$). The order $2p+1$ truncation errors are much more accurate than at other points on the cell, a fact demonstrated before in Refs. [33,34] (where it was also shown for the cell average). For this reason, it has been termed superconvergence.

MAPLE can also be used to produce an estimate of the local truncation error on a cell once the high order methods have been computed with the Galerkin procedure. For a cell i and angle μ_m, the non-dimensional cell parameter h, or optical thickness, is

$$h = \frac{\Delta x_i \, \sigma_{ti}}{\mu_m},$$

and the exact solution for the outgoing flux ψ_{out}, given an incoming flux ψ_{in}, in a source free, purely absorbing, medium is given in terms of the cell parameter simply as $\psi_{\text{out}} = \psi_{\text{in}} \, e^{-h}$. We can similarly write the numerical approximation to the outgoing flux as a function of the optical thickness in terms of the incoming flux (the outgoing flux from the previous cell as described above) and a sum over the scattering source moments s_n (which are zero in a source and scattering free medium):

$$\psi_{\text{out}} = \psi_{\text{in}} f_p(h) + \sum_{n=0}^{p} g_{pn}(h)\, s_n. \tag{19}$$

The functions $f_p(h)$ for $p = 1 \ldots 6$ are

$$f_1(h) = \frac{-2h + 6}{h^2 + 4h + 6} \tag{20a}$$

$$f_2(h) = \frac{3h^2 - 24h + 60}{h^3 + 9h^2 + 36h + 60} \tag{20b}$$

$$f_3(h) = \frac{-4h^3 + 60h^2 - 360h + 840}{h^4 + 16h^3 + 120h^2 + 480h + 840} \tag{20c}$$

$$f_4(h) = \frac{5h^4 - 120h^3 + 1260h^2 - 6720h + 15120}{h^5 + 25h^4 + 300h^3 + 2100h^2 + 8400h + 15120} \tag{20d}$$

$$f_5(h) = \frac{-6h^5 + 210h^4 - 3360h^3 + 30240h^2 - 151200h + 332640}{h^6 + 36h^5 + 630h^4 + 6720h^3 + 45360h^2 + 181440h + 332640} \tag{20e}$$

$$f_6(h) = \frac{7h^6 - 336h^5 + 7560h^4 - 100800h^3 + 831600h^2 - 3991680h + 8648640}{h^7 + 49h^6 + 1176h^5 + 17640h^4 + 176400h^3 + 1164240h^2 + 4656960h + 8648640}. \tag{20f}$$

As is usually done, these functions may be expanded in a Taylor series in the parameter h and compared to the Taylor series expansion of the exponential function to estimate the order of the truncation error. The expansions should agree up to the term containing h to the power $2p + 1$. The next terms of the expansions, containing one higher power in h, will have different coefficients. In Table 1 we list the first terms of the expansions that differ for the cases $p = 1 \ldots 6$, confirming order $2p + 1$ convergence rate.

Similar expansions can be computed for the cell average flux, other spatial moments of the flux, the fluxes at the knots of the cell, and the source moment functions $g_{pn}(h)$, all quite easily using MAPLE.

We now consider the stability and positivity characteristics of the methods. Following the work of Germogenova, et al.,[10] the functions $f_p(h)$ for values of $p = 1 \ldots 6$ are plotted in Fig. 2. They are seen to closely approximate the exponential function reflecting the fact that the numerical methods actually generate rational polynomial (Padè) approximations to the exponential. This is not surprising since the Padè representation is defined by

Table 1 Convergence Rates for the Degree p Polynomial Approximations.

p	Convergence order	Lagrange approximation	Exponential function
1	3	$\frac{1}{36}h^4$	$\frac{1}{24}h^4$
2	5	$\frac{11}{7200}h^6$	$\frac{1}{720}h^6$
3	7	$\frac{17}{705600}h^8$	$\frac{1}{40320}h^8$
4	9	$\frac{127}{457228800}h^{10}$	$\frac{1}{3628800}h^{10}$
5	11	$\frac{461}{221298739200}h^{12}$	$\frac{1}{479001600}h^{12}$
6	13	$\frac{1717}{149597947699200}h^{14}$	$\frac{1}{87178291200}h^{14}$

the order to which it agrees with the original function, in this case the source and scattering free solution, e^{-h}.

It can be implied from the figure that the S_N source iterations are stable, since $|f_p(h)| < 1$ for all h, $f_p(h) \to 0$ as $h \to \infty$, and $f_p(h) \to 1$ as $h \to 0$. MAPLE was used to confirm this using the following iteration matrix formulation. A step of the S_N spatial march, say for $\mu > 0$, can be written as

$$\overline{\psi}_i = \mathbf{A}^{-1}\mathbf{B}\overline{\psi}_{i-1}$$

where $\mathbf{A}$ is the coefficient matrix for the cell and the vector $\overline{\psi}_i$ contains the cell coefficients of the Lagrange expansion, $\{\psi_n\}_{n=0}^{p}$. The matrix $\mathbf{B}$ picks out multiples of certain elements of the flux vector from the previous cell. A method is stable if the norm $||\mathbf{A}^{-1}\mathbf{B}|| < 1$. It turns out that the norms for the high order methods, which depend on the cell parameters and hence on h, are in fact bounded by the functions $f_p(h)$. This approach facilitates similar analysis of high order methods in higher dimensions.

Interestingly, it can be seen that for p odd these functions are not positive over the entire range of h, while for p even they are. This is a significant result since so much effort has been given to producing positive schemes out of inherently negative methods such as the diamond difference and linear discontinuous methods.[9] However, positive outgoing fluxes cannot be guar-

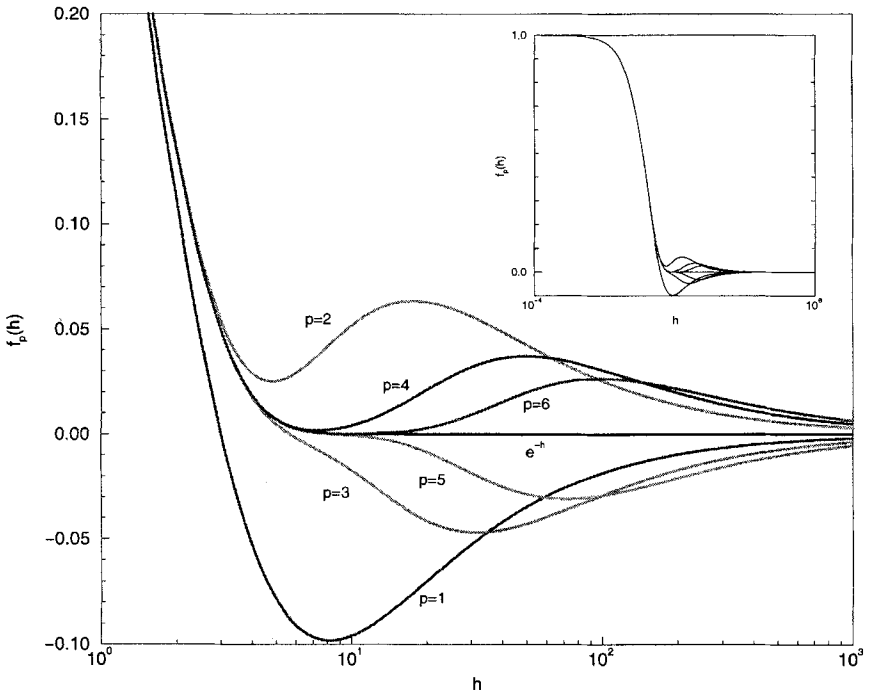

Figure 2

Plots of the functions $f_p(h)$ for $p = 1..6$. The exponential function e^{-h} is also shown. The numerical solutions approximate the exponential function as expected, and asymptotically approach it (inset) for both large and small values of the cell parameter h.

anteed, even for isotropic scattering, because the source moment functions $g_{np}(h)$ in Eq. 19 can be negative over a wide range of h. Still, the positivity of the $f_p(h)$ functions, or lack of same, has a strong impact on the overall positivity of the numerical methods. The methods have a tendency to produce negative fluxes any time the cell parameter h exceeds the real zero of the function $f_p(h)$. The zeros have been computed symbolically with MAPLE and we find that for p odd $f_p(h)$ has one real zero, the rest being complex conjugate pairs, while for p even the zeros are all complex conjugate pairs, and we make the conjecture that this pattern continues. This explains the positivity of the p even cases.

Hennart and del Valle point out in Ref. [13] that continuous methods, such as the diamond-difference scheme, correspond to diagonal Padè approximants (where the rational approximation to the exponential contains the same highest power of h in both the numerator and denominator) which display a false asymptote $f_p(h) \to (-1)^p$ for large h. They further note that the discontinuous methods (they show only the LD method) correspond to the sub-diagonal Pade approximants (one higher power of h in the denominator than in the numerator, as seen in Eqs. 20) which have the correct asymptotic behavior. What is not indicated is that the discontinuous methods show an alternating pattern of positivity that depends on the parity of the degree of the approximating polynomial representation. These facts have implications for the adaptive implementation of the high order methods.

3. p-ADAPTIVE IMPLEMENTATION

The high order schemes have been implemented in an adaptive way starting with the source code for the high-order polynomial representations, $p = 1 \ldots 6$, generated using the computer algebra program MAPLE. Special consideration is given to implementing the S_N source iterations.

An adaptive step proceeds as follows. Given some scattering source (initially 0.0 for the first S_N iteration) and an incoming flux for the cell, along with the cell parameters, the outgoing flux is computed for for $p = p_{\min}$ and also for $p = p_{\min} + 1$ (the factors influencing the choice of the minimum degree $p_{\min}$ will be discussed below). If these do not agree to some specified tolerance, then the outgoing flux for the next order is computed and compared to that from the previous order. Of course the average flux or other sensible quantity could be used as the standard of comparison. The process of increasing the degree of the polynomial representation, and hence the accuracy of the approximation, continues until the tolerance is satisfied (by the maximum of the absolute and relative errors) or until the computations have reached the maximum degree $p = p_{\max}$ ($p_{\max} = 6$ in the current implementation). The process also terminates when and if the computed outgoing flux is zero, regardless of the current value of p.

The highest order representation used on a cell in an adaptive step will vary from one S_N iteration to the next. This does not appear to ad-

versely affect the convergence rate. Rather, the higher order accuracy of the p-adaptive method seems to improve convergence in the sense that the number of iterations reaches an asymptotic limit, based on the spectral radius, on a coarser mesh than do the non-adaptive schemes.

It is not necessary to start the adaptivity with $p_{\min} = 1$, because it is possible with MAPLE to easily use any value of $p_{\min}$. In light of the positivity of the even order methods, we believe it is sensible to start with $p_{\min} = 2$ rather than with $p_{\min} = 1$ despite the increased computational demand. This choice was seen to dramatically improve the positivity of the adaptive method solutions, although the capability to use either minimum representation was retained and results of both are reported for the numerical experiments shown in the next section.

At the end of an adaptive step, the flux coefficients for the highest degree of approximation computed are used to find the average flux. "Effective" $p = p_{\min}$ fluxes are then also computed to which the scattering operator is applied for every mesh cell in order to generate a $p_{\min}$ scattering source for the next iteration. Similarly, the source moments appropriate for any value of p in an adaptive step greater than $p_{\min}$ can be computed using the "scattered" order $p_{\min}$ fluxes. MAPLE is used to symbolically compute these projections as discussed below.

The "effective" $p = p_{\min}$ fluxes are computed by projecting the degree p solution onto the $p_{\min}$ representation as follows. First, assume that we have computed the fluxes for a $p > p_{\min}$ flux representation, designated $\tilde{\psi}_p(x)$. We take the inner products of this with the $p = p_{\min}$ basis functions, $L_k^\star(x), k = 0 \ldots p_{\min}$, and set the "effective" $p_{\min}$ source terms

$$s_0^\star =< L_0^\star(x) \mid \tilde{\psi}_p(x) >$$

$$\vdots$$

$$s_{p_{\min}}^\star =< L_{p_{\min}}^\star(x) \mid \tilde{\psi}_p(x) >, \tag{21a}$$

where the superscripts * are meant to make a distinction between the order $p_{\min}$ Lagrange basis functions and source terms and those used in the order p representation.

We can then solve the $(p_{\min}+1 \times p_{\min}+1)$ system of equations

$$s_0^\star =< L_0^\star(x) \mid L_0^\star(x) > \psi_0^\star + \ldots + < L_0^\star(x) \mid L_{p_{\min}}^\star(x) > \psi_{p_{\min}}^\star$$

$$\vdots$$

$$s_{p_{\min}}^\star =< L_{p_{\min}}^\star(x) \mid L_0^\star(x) > \psi_0^\star + \ldots + < L_{p_{\min}}^\star(x) \mid L_{p_{\min}}^\star(x) > \psi_1^\star \quad (21b)$$

for the "effective" fluxes $\left\{\psi_n^\star\right\}_{n=0}^{p_{\min}}$.

The $p = p_{\min}$ scattering source is calculated according to the S_N angular discretization using these "effective" fluxes, that is, after each iteration the scattering operator is applied to the fluxes: $\left\{\hat{S}\psi_i^\star\right\}_{i=0}^{p_{\min}}$. These are used directly as source terms for the initial $p_{\min}$ adaptive step on a mesh cell. For $p > p_{\min}$, the $p_{\min}$ scattering source terms are projected onto an order p representation by evaluating the expressions

$$s_k =< L_k(x) \mid L_0^\star(x)\hat{S}\psi_0^\star > + \ldots$$
$$\ldots + < L_k(x) \mid L_{p_{\min}}^\star(x)\hat{S}\psi_{p_{\min}}^\star >, \quad k = 0 \ldots p. \quad (22)$$

The expressions in Eqs. 21 and 22 are evaluated symbolically using MAPLE and the source code for $p = p_{\min} \ldots 6$ is produced automatically.

4. NUMERICAL RESULTS

We now present results obtained with the high order and p-adaptive schemes. Several types of problems are solved, and some are taken to make connection with previous investigations in the literature. Isotropic scattering is assumed and, unless otherwise noted, the S_N source iterations are converged to 10^{-5} on the cell average scalar fluxes. The p-adaptive tolerance depends on the problem and is selected on a case-by-case basis. If not specified, $p_{\min} = 2$ is used for the adaptive methods.

Problem 1 is a homogeneous medium with a beam source of strength 48 cm^{-2} s^{-1} normally incident on the left face a 16.0 cm slab with a vacuum boundary condition on the right. A first-scattered distributed source technique is used to model the incident beam. The interaction cross sections are $\sigma_s = 14.0$ cm^{-1} and $\sigma_a = 2.0$ cm^{-1}, so the slab is 256 mean free paths (mfp) thick. We use $N_x = 16$ mesh cells and an S_8 quadrature. The p-adaptive tolerance is set to $4 \cdot 10^{-3}$. The solutions for various orders of p as well as the adaptive method with $p_{\min} = 2$ are shown along with the diamond-difference method in Fig. 3. The latter exhibits severe oscillations

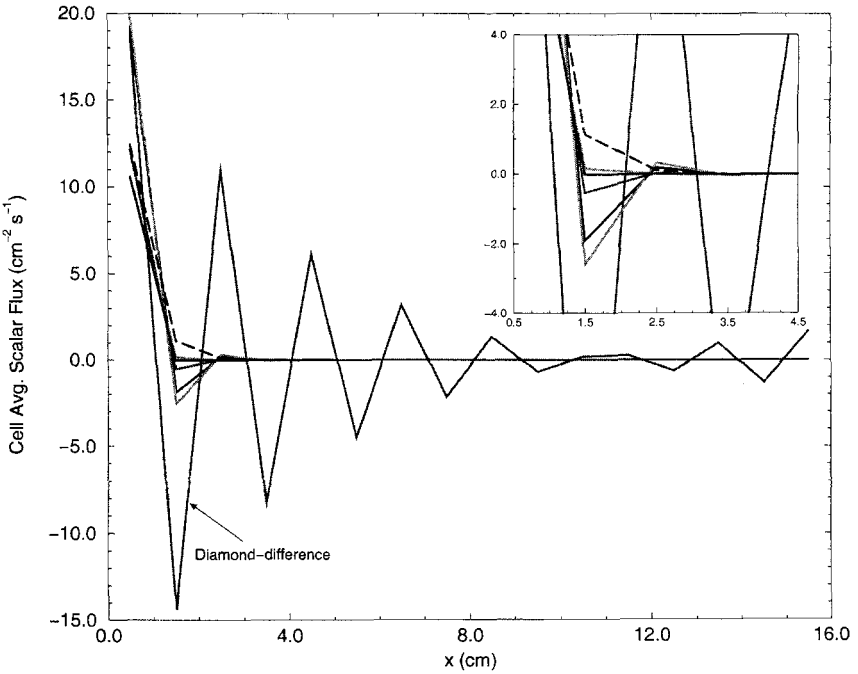

Figure 3

Plot of the scalar flux in Problem 1. The inset shows the negative fluxes produced by the high order methods with p odd.

and negative fluxes (no negative flux fixup was used). The inset shows that the high order methods with p odd drop below zero in the second mesh cell. While it is not clear from figure (because the fluxes drop off so quickly with distance), the methods never recover. The p odd methods produce fluxes that alternate between positive and negative from cell to cell, whereas the fluxes computed by the adaptive method and the methods with p even are monotonic and positive.

The next results are for a similar problem, except that the scattering cross section is 12.0 cm^{-1}, the absorption cross section is 1.0 cm^{-1}, and the first-scattered distributed source option is not used.

We trace how the p-adaptive method with $p_{\min} = 2$ progresses through the S_N iterations in Fig. 4. Each of the four plots, one for each of four

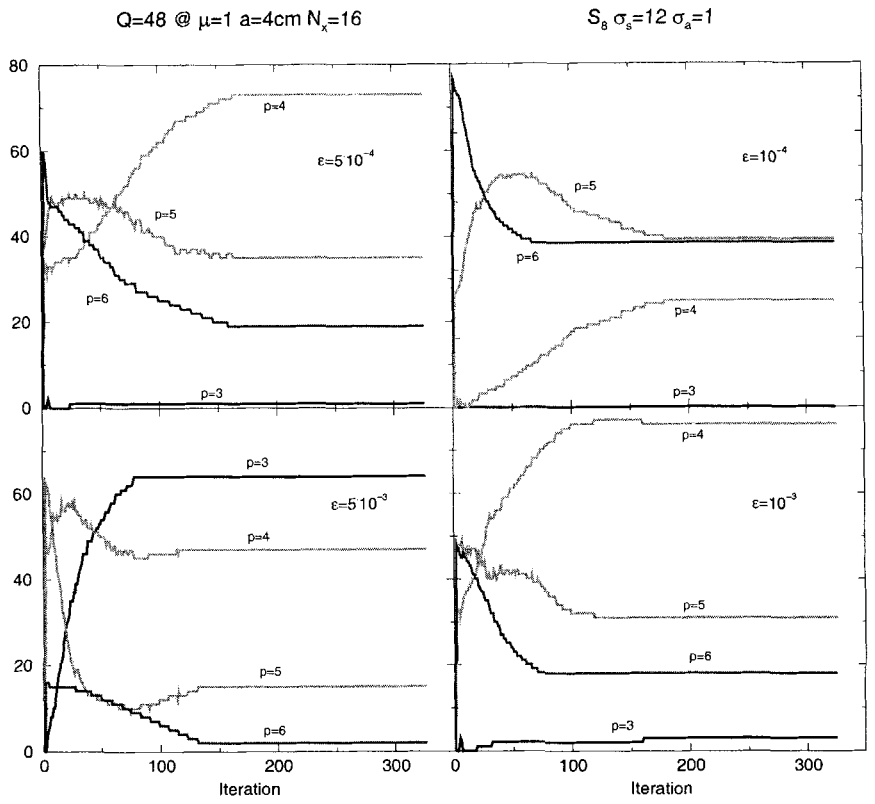

Figure 4

Plot of the p-adaptive method progression through the S_N source iterations for various values of the adaptive tolerance ϵ.

different values of the adaptivity tolerance, show the total number of angular flux computations that required an order p calculation at each iteration, one for every cell and every angle. For the 16 spatial meshes in this problem and an S_8 quadrature, there is a total of 128 calculations at each iteration. The curve for $p = p_{\min}$ is not shown because the only time the adaptive step terminates at $p_{\min}$ is when the outgoing flux is zero (as it is for the first iteration which is not shown); otherwise, both the $p_{\min}$ and $p_{\min} + 1$ fluxes are computed and the $p_{\min} + 1$ values, at a minimum, are used for

the next step. The plot shows the evolution of the adaptivity to a final steady state that continues until the source iterations converge. Decreasing the tolerance on the outgoing fluxes for the adaptive steps increases the number of computations that need a higher order representation to meet the tolerance. The adaptivity progression is not greatly affected by the choice of $p_{\min}$, but the $p_{\min} = 1$ and $p_{\min} = 2$ results differed dramatically their positivity.

At the conclusion of the S_N iterations the values of the flux at the cell knots for the polynomial representation used during the final iteration can be printed for each mesh cell and for every angular index. Together with the Lagrange basis function representation they can be used to reconstruct the angular flux in the mesh. We show in Fig. 5 two such flux reconstructions for symmetric forward and backward directions in the central mesh cells of Problem 1 at two levels of spatial discretization, $N_x = 8$ and $N_x = 16$. The p-adaptive tolerance is 10^{-3}. For the coarser mesh, discontinuities at the cell edges and rapid oscillatory variation within the cells are clearly evident, and are seen to diminish as the mesh is refined.

The next problem is one originally used by Reed[36] and subsequently by several others (see Refs. [9, 10, 12, 13, 21]). It consists of a heterogeneous medium with five regions and four different materials, some containing isotropic external sources. There are $N_x = 40$ equally spaced mesh intervals and an S_8 quadrature is used. The p-adaptive tolerance is set to 10^{-6}. We refer to this as Problem 2; geometry and material properties are shown in Table 2.

This problem provides a stringent test for a numerical method, and highlights the weaknesses of the diamond-difference methods. Martin and Duderstadt[21] point out that it is the presence of the void region next to the region of high absorption that causes discontinuities in the angular flux. The backward-directed fluxes attempt to match the source in region 1 from an effectively zero flux in the absorptive region 2. A similar situation occurs for the forward-directed fluxes from the void in region 3 to the source in region 4, although to a lesser extent. Imposing continuity on the flux at the interfaces causes oscillations, as illustrated in Fig. 6, for the diamond-difference schemes. The discontinuous spatial discretizations do much better. The

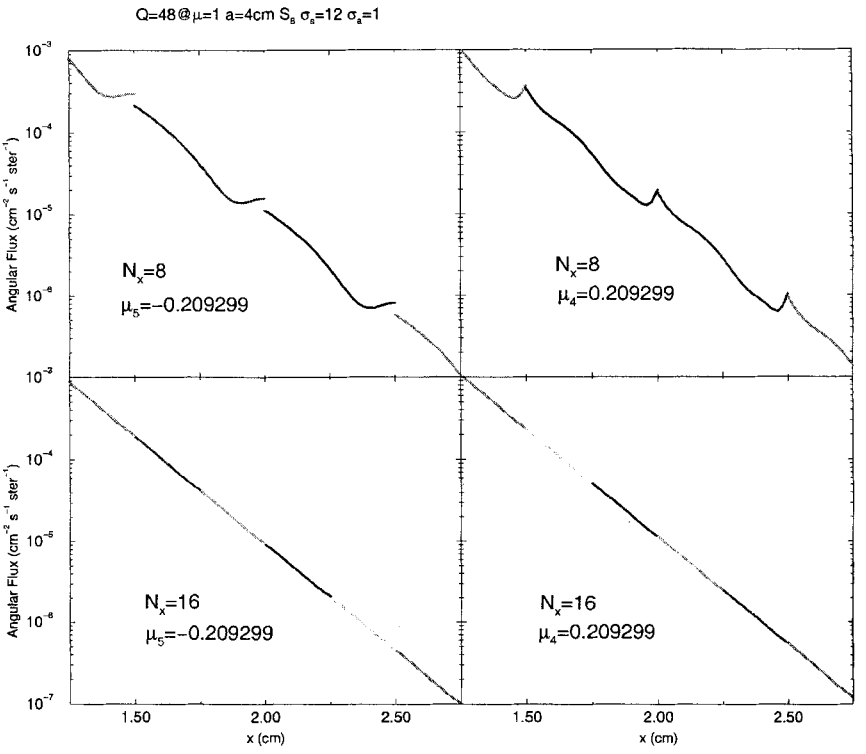

Figure 5

Plot of the reconstructed angular fluxes for backward and forward directions using an S_8 quadrature with two levels of spatial discretization.

Table 2 Geometry and Material Properties for Problem 2.

Region:	1	2	3	4	5
x (cm)	0.0–2.0	2.0–3.0	3.0–5.0	5.0–6.0	6.0–8.0
σ_s (cm^{-1})	0.00	0.00	0.00	0.90	0.90
σ_a (cm^{-1})	50.0	5.00	0.00	0.10	0.10
Q (cm^{-3} s^{-1})	50.0	0.00	0.00	1.00	0.00

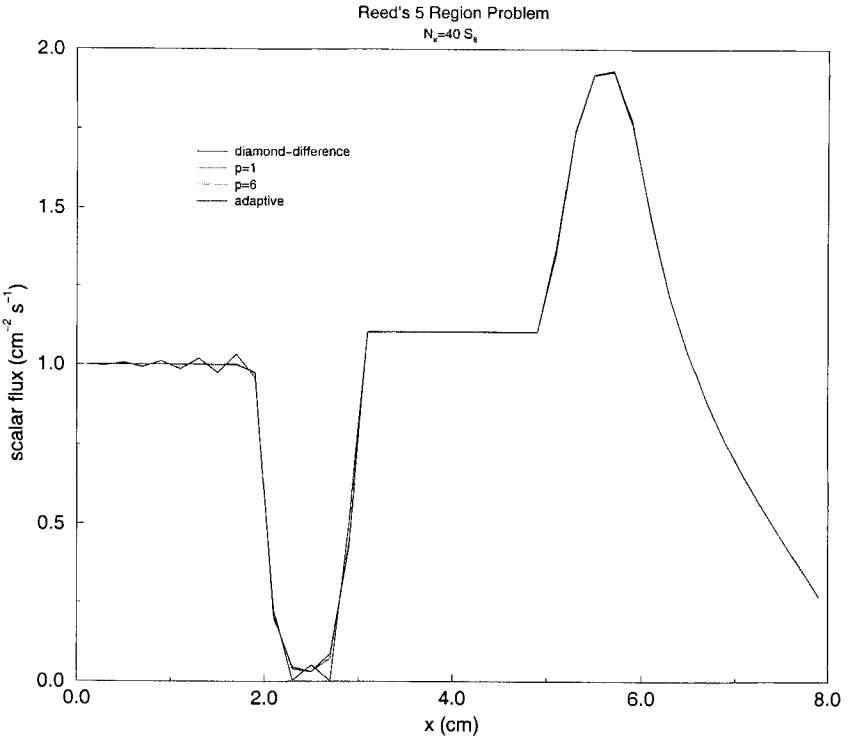

Figure 6

Plot of the scalar flux in the five region heterogeneous medium of Problem 2. Some oscillations appear in the diamond difference solution.

steep flux gradient means that the fluxes near the absorbing region 2 to region 1 always require a high order computation, regardless of the tolerance. In Table 3 we show the final order used in the adaptive computation for the mesh cells near region 2 for each of the angular ordinates. This is also graphically illustrated in Fig. 7, where some of the reconstructed fluxes near this region are shown for two symmetric forward and backward directions. The pronounced discontinuities and high order oscillations in the computed flux are clearly seen for the backward fluxes as the method attempts to match fluxes at the interface. The forward fluxes show little discontinuity,

Table 3 Final Degree of Approximation Used on the Mesh Near the Region of Absorption in Problem 2.

x range (cm)	μ_1 -1.0000	μ_2 -0.8717	μ_3 -0.5917	μ_4 -0.2093	μ_5 0.2093	μ_6 0.5917	μ_7 0.8717	μ_8 1.0000
1.4 – 1.6	3	3	3	6	3	3	3	3
1.6 – 1.8	5	6	6	6	3	3	3	3
1.8 – 2.0	6	6	6	6	3	3	3	3
2.0 – 2.2	4	5	5	6	6	5	5	4
2.2 – 2.4	4	5	5	6	6	5	5	4
2.4 – 2.6	4	5	5	6	6	5	5	4
2.6 – 2.8	4	5	5	6	6	5	5	4
2.8 – 3.0	4	5	5	6	6	5	5	4
3.0 – 3.2	3	3	3	3	3	3	3	3
3.2 – 3.4	3	3	3	3	3	3	3	3

if any, but a high order representation is still needed to satisfy the high absorption in region 2.

We also investigated the accuracy of the p-adaptive method using a MAPLE implementation of the analytical S_N solution from Davison.[38] Angle-integrated quantities are considered since these are typically most important for applications. We derived expressions for the S_8 angular fluxes which were used to evaluate the cell-averaged scalar flux and slab currents. While 25 digits of precision in software were retained, the point-wise scalar fluxes for both this problem and the next are shown in the appendix to about 15 significant digits. The analytical expressions are used to determine the error in the numerical solution, eliminating any dependence on the S_N approximation. There is one caveat: the high order methods are very accurate even on coarse meshes, so much so that the level of error in the spatial discretization may fall below that of the source iteration tolerance and a very low S_N tolerance may be required. We used 10^{-12} for this problem.

In Fig. 8 we show the error in the computed scalar fluxes relative to the analytical solution as the adaptivity tolerance is decreased. Below about

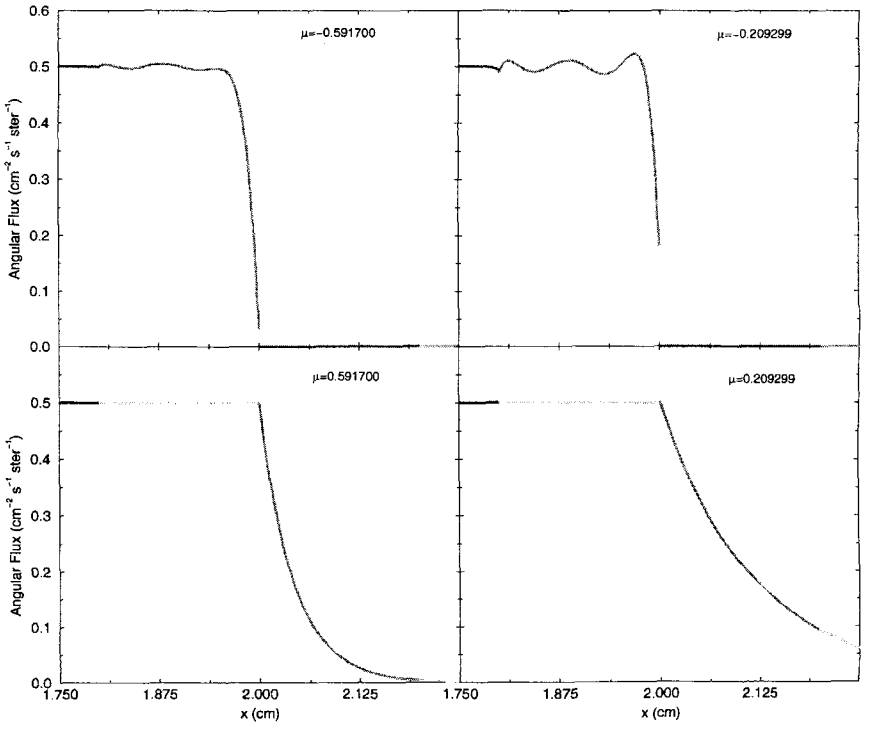

Figure 7

Angular fluxes for selected angles near the region of high absorption in Problem 2.

10^{-6} there is not much influence on the level of adaptivity or the relative errors with the current value of $p_{\max} = 6$. Around the absorbing region, region 2, and to a lesser extent near the source region in region 4, a good deal of adaptation takes place. Decreasing the adaptive tolerance is seen to improve the local accuracy of the computation in these areas on a fixed, fairly coarse mesh. Away from these regions, the local error is less affected by and less sensitive to the level of adaptivity. For a tolerance of about 10^{-3} the minimum order is used on most of the mesh. As the the adaptive tolerance is decreased, increasingly higher order computations are required throughout the mesh with little local improvement in accuracy. The adaptive tolerance must be selected carefully.

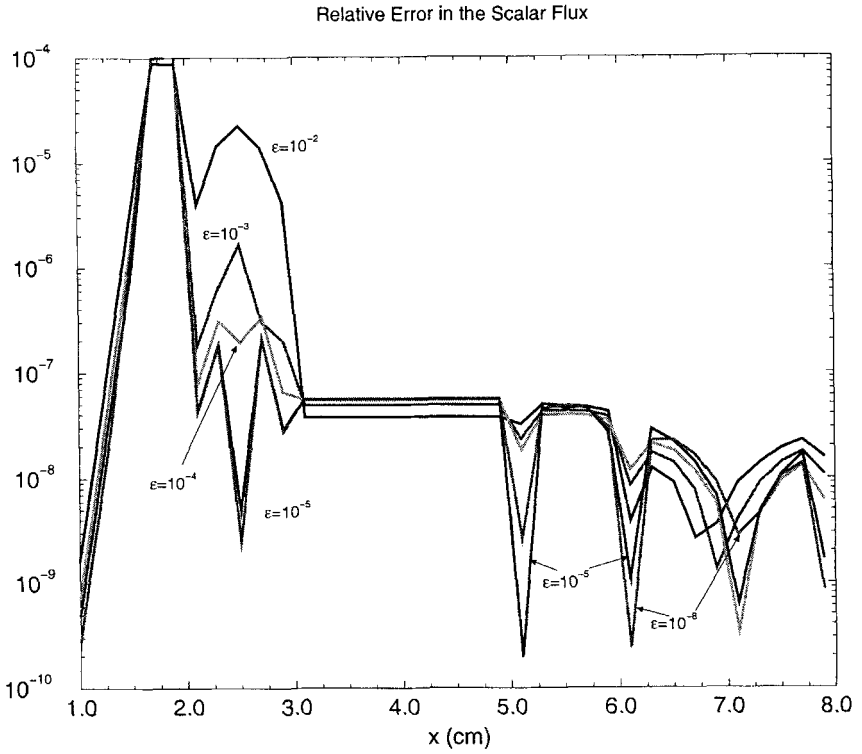

Figure 8

Relative error in the cell-average scalar flux across the mesh for Problem 2. The result for several values of the adaptivity tolerance ϵ is shown.

The next problem, Problem 3, is taken from Mathews, et al.[37] For an isotropic boundary source on the left face of the slab and vacuum condition on the right, the analytical S_8 solution in a homogeneous 32 mfp thick slab and a total cross section of unity was used to get a sense of the global accuracy of the p-adaptive methods. Following Mathews, we consider the two scattering ratios, $c = 0.9$ and $c = 0.1$. We use the L_1 norm of the difference between the computed and exact cell-average scalar fluxes on the mesh, ϕ_i and ϕ_i^{exact}, respectively, as a measure of error, defined as

$$\frac{1}{N_x}\sum_{i=1}^{N_x}\left|\phi_i - \phi_i^{\text{exact}}\right|. \tag{23}$$

To observe the expected spatial discretization convergence orders on fine meshes, as noted, we use S_N tolerances that are quite small, 10^{-13} for this problem. In fact, agreement to full machine precision was achieved on meshes with cells as thick as $\frac{1}{4}$ mfp for the order $p = 5$ and 6 methods.

In the following figures, the curves labeled $p_{\min} = 1$ and $p_{\min} = 2$ are for the two adaptive methods, and the other curves are for the fixed high order methods of degree p. The L_1 error in the scalar flux is shown for the case $c = 0.9$ in Fig. 9 as a function of the number of mesh cells. Assuming that the flux is not zero, the minimum order for which an adaptive step terminates is the $p_{\min} + 1$ computation. Hence, the overall error is expected to be somewhere between this and the order used for the source iteration representation, $p_{\min}$. The figure shows this to be the case. The curve for the $p_{\min} = 2$ adaptive method lies between the $p = 2$ and $p = 3$ curves, and that of the $p_{\min} = 1$ lies between those for $p = 1$ and $p = 2$. For this case, this is insensitive to the adaptive tolerance.

The reflected current at $x = 0$ is computed as

$$J^- = \sum_{\mu_m<1} w_m\mu_m\psi_m(0). \tag{24}$$

We show in Fig. 10 the absolute error in this quantity for the various methods relative to the exact value of 0.49129461334888 $\text{cm}^2\ \text{s}^{-1}$ as a function of the number of mesh cells. We also have included the results of the diamond-difference computation (labeled "DD") which, as pointed out by Mathews, is extremely accurate even on a fairly coarse mesh and which he attributes to cancellation errors. The curves for this and the high order methods are terminated for meshes where the computed and exact values of the current agreed to machine precision, about 14 digits. The $2p + 1$ convergence rates should apply to this quantity since the negatively directed cell edge angular fluxes on the left (outgoing) side of the first mesh cell are used to compute the numerical result. For fine enough meshes, that is, for cells less than about 2 mfp thick, they are in agreement with the stated $2p + 1$ convergence order. A linear fit to the log-log curves of the $p_{\min} = 2$ adaptive method

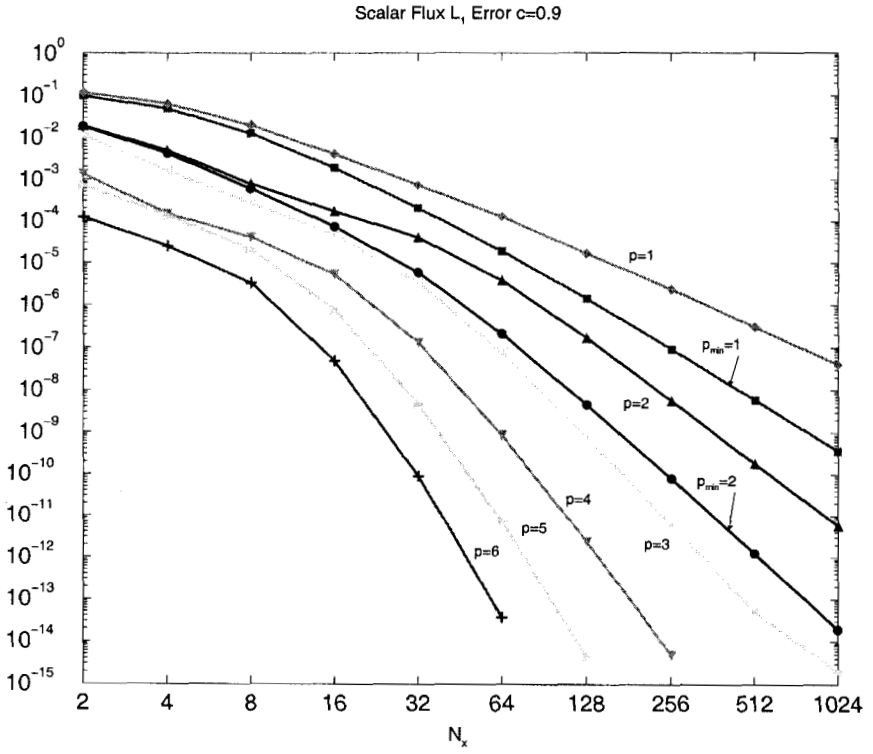

Figure 9

Plot of the L_1 error norm of the cell-average scalar fluxes for Problem 3 with $c = 0.9$ as a function of the number of mesh cells, N_x.

error gives a slope of approximately -5.860 or an order of accuracy of about 6. For the $p_{\min} = 1$ methods, the slope is estimated to be -3.924, very close to a convergence rate of 4.

The L_1 error in the scalar flux is shown in Fig. 11 for $c = 0.1$, a streaming dominated problem. The adaptivity tolerance is again 10^{-6}. The accuracy of the p-adaptive methods for thick cells is much improved over those for the case $c = 0.9$. Both of the p-adaptive methods show an accuracy comparable to that of the highest order methods. For thin cells, though, the error again lies between the order $p_{\min}$ and order $p_{\min} + 1$ methods. Since this problem

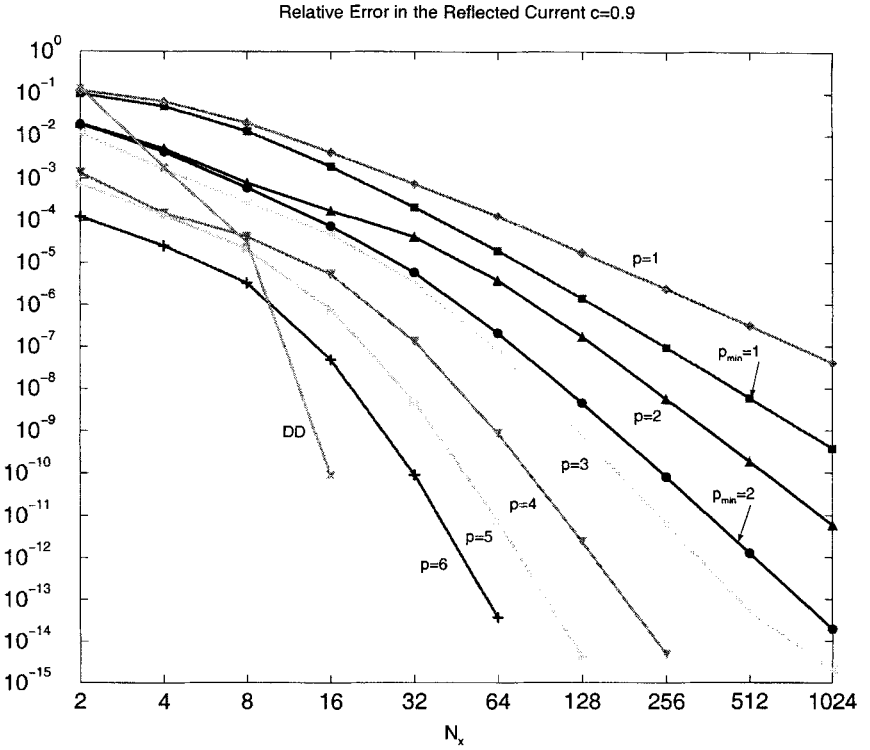

Figure 10

Relative error in the current reflected from a 32mfp thick slab with $c = 0.9$ as a function of the number of mesh cells, N_x.

involves very little scattering and the results are again insensitive to the adaptive tolerance, the global error must therefore depend strongly on the scattering source representation. The coarse meshes require adaptation to high order, regardless of the tolerance, and the small scattering ratio means that the source representation does not dominate the global error.

Since this is a streaming-dominated problem, we compute the relative error in the transmitted current for this case, that is,

$$J^{+} = \sum_{\mu_m > 0} w_m \mu_m \psi_m(32). \tag{25}$$

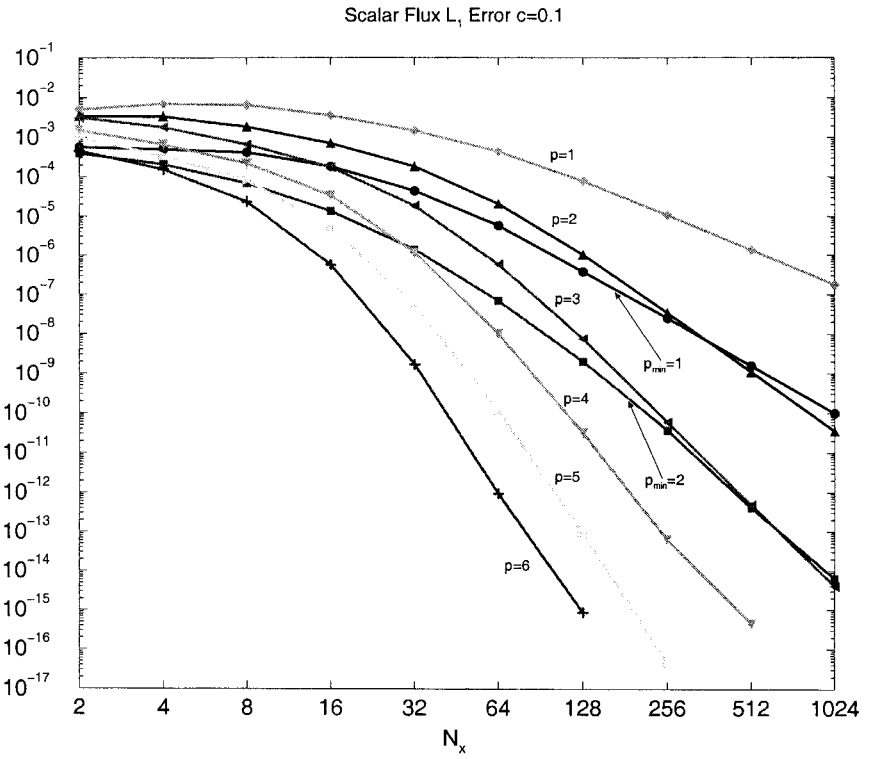

Figure 11

The L_1 error in the cell-average scalar fluxes for Problem 3 with $c = 0.1$ as a function of the number of mesh cells, N_x.

The exact value to 14 significant digits is $0.12889276627254 \cdot 10^{-14}$ cm^2 s^{-1}. Fig. 12 shows that for thick cells all the methods err by many orders of magnitude. We can estimate the order of accuracy of the adaptive methods for fine meshes (cells less than 4 mfp thick) from this figure. The $2p + 1$ convergence rates should again apply to this quantity, as for the reflected current in the $c = 0.9$ case, because this time the positively directed cell edge angular fluxes on the right side of the last cell are used to compute the numerical result. Linear regression of the log-log curves estimate a slope of -4.005 for the $p_{\min} = 1$ adaptive method, and a slope of -5.892 for

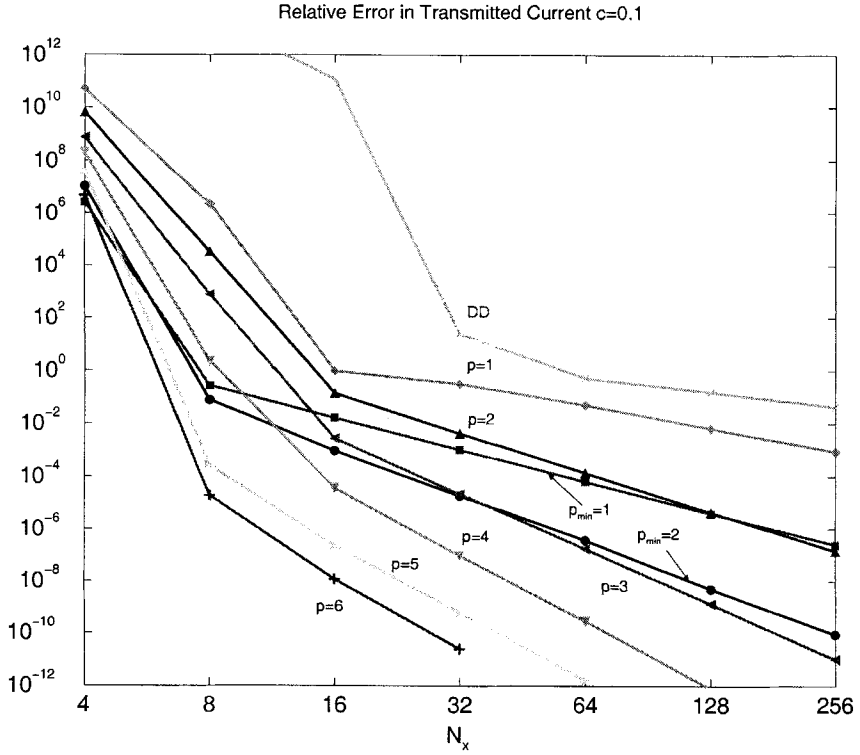

Figure 12

Relative error in the transmitted current exiting a 32mfp thick slab with $c = 0.1$ as a function of the number of mesh cells, N_x. The curves labeled "$p_{\min} = 1$" and "$p_{\min} = 2$" are the adaptive methods.

$p_{\min} = 2$, so that the order of accuracy is about 4 and 6, respectively. They agree with the results of the $c = 0.9$ case.

The slopes of the L_1 errors in the scalar flux in Figs. 9 and 11 were used to estimate the global order of the truncation error for the adaptive methods. In accordance with the superconvergence properties of the discontinuous methods, the order $2p+1$ convergence rate applies to the cell-average fluxes, so they should also apply to the cell-average scalar fluxes for the fixed order methods. The *p*-adaptive methods depend on the level of scattering in the

Table 4 Estimated Order of Accuracy for Problem 3.

Method	$c = 0.9$	$c = 0.1$
$p = 1$	2.903	2.834
$p = 2$	4.844	4.812
$p = 3$	6.425	6.810
$p_{\min} = 1$	3.924	3.954
$p_{\min} = 2$	5.860	5.900

problem, but are be bounded by the order used to for the source projections, $p_{\min}$, and the next highest order, $p_{\min} + 1$.

In the Table 4, we list the orders of accuracy estimated with a linear regression of the L_1 log-log errors for cells thinner than 1 mfp for both $c = 0.1$ and $c = 0.9$. These results are in good agreement with the theoretical $2p+1$ truncation errors and indicate that the global order of accuracy of the adaptive methods are in fact bounded by the $p_{\min}$ and $p_{\min} + 1$ representations.

It is important to note that truncation error analysis only applies in the limit of diminishing cell thickness. This is illustrated in the plot of the errors in the transmitted current, Fig. 12, where the asymptotic behavior is very evident. That is why the convergence rates can be stated only for meshes which are fine enough in this asymptotic sense.

Finally, the p-adaptive method was also tested for the anisotropic iron-water problem in Ref. [8] (also considered in Ref. [23]) to see if anisotropic scattering presented any unforeseen difficulties. There was clearly no difficulty in doing so.

5. SUMMARY AND FUTURE WORK

We have implemented and tested a p-adaptive transport method and demonstrated that in certain situations it exhibits better numerical properties than the commonly used low order diamond-difference and linear-discontinuous methods.

The p-adaptive method produces numerical solutions with improved accuracy, although we emphasize it is very much a local effect. It appears that the global accuracy is bounded by that of the polynomial degree used for the source representation of the S_N source iterations, $p_{\min}$, and the minimum order of computation used in an adaptive step, $p_{\min} + 1$. This is true in an asymptotic sense: the truncation error order of $2p + 1$ applies as the mesh cell optical thickness becomes small. The accuracy for thick cells, or in the diffusion limit, awaits further anlaysis. Still, it was seen that for coarse meshes the global accuracy is improved through adaptation to higher order, but this improvement is limited by the projective method used to implement the source iterations. In a highly scattering medium the overall accuracy tends to be reduced to that of the minimum source representation, whereas if the medium is absorptive, the global accuracy tends to be dominated by the highest order needed to satisfy the adaptive tolerance. Angle-integrated quantities are more susceptible to a reduction in accuracy because they are evaluated by a sum of angular fluxes of differing accuracies.

However, high order computations are made only where necessary and, for heterogenous media in particular, a real improvement in accuracy can be achieved on a local basis. This depends to a large extent on the adaptivity tolerance and is true as long the tolerance is not so low that high orders are used througout the mesh. In order to avoid wasted computation, this parameter must be carefully selected by monitoring the level of adaptivity taking place or by making error estimates (with successive mesh refinement, for example).

Local improvement in accuracy of the angular flux leads to improved global positivity. Since actual solutions to the transport equation (in both a physical and analytical sense) are necessarily positive, more accurate numerical solutions are presumably closer to this solution and thus are more likely to be positive. Also, the higher order, locally positive solutions carry through to the rest of the mesh during the course the spatial march and the S_N source iterations. Computing angular fluxes which are positive will improve the positivity of the scalar flux as well, which is very desirable. Using a minimum order of $p_{\min} = 2$, which tends to give positive solutions, was also seen to improve the overall positivity. This is also true for the fixed high order methods and especially on coarse meshes.

Although we have not explored just how much cost is incurred in achieving these attributes, the p-adaptive method is surely more complex and therefore requires more computation for a given level of accuracy than the fixed order methods. However, work in progress indicates that the computational efficiency could be improved using a hierarchic functional representation.[29–31] Under the current formalism, using the Lagrange polynomials, an adaptive step requires that a complete set of flux coefficients be computed each time the polynomial degree is incremented. With the hierarchic functions, the equations for each coefficient are de-coupled. Thus, for every degree of approximation only the next flux coefficient needs to be computed; the values of the previously computed coefficients are unchanged and can be reused. Even if a set of basis functions is used for which there is not a complete de-coupling, it may be possible to produce equations which are only partially coupled (a sparse matrix), for which the expressions for the cell flux coefficients would be less complicated and less costly to compute or perhaps enabling the partial reuse of lower order coefficients.

There other opportunities for possibly increasing the computational performance of the p-adaptive method, including reversing the order of the spatial march and angular sweep and adapting based on the scalar flux, using a single order method to compute all the angular fluxes on a cell in an adaptive step. Another might be the implementation of the commonly used Diffusion Synthetic Acceleration (DSA) technique for accelerating the source iterations of the S_N method.

If an adaptive method is to have the potential for use in a production code environment, it is imperative that the source iterations are accelerated. It has been noted[23,39] that the discretization of the low order operator, used to attenuate the low frequency error modes, must be consistent with the discretization of the high order operator. In the case of DSA, the low order operator is the diffusion equation and the high order operator is the transport equation itself. The diffusion equation could be discretized in the same manner as the $p_{\min}$ representation of the angular flux in the S_N equations. That is, a $p_{\min}$ Lagrange polynomial approximation can be used for the scalar flux and the Galerkin procedure applied to the corresponding diffusion equation, again using MAPLE. The zeroth and first scalar flux

moments of the "effective" $p_{\min}$ transport fluxes could be accelerated at each iteration using fluxes from the previous iteration to compute the source term for the diffusion equation solution.

Based on the investigation of the *p*-adaptive method in one dimension it is proposed to apply the method to more complicated transport regimes. The method could be extended to two or three-dimensional geometry or to problems with energy dependence. There exist applications in both situations for which adaptivity could provide greater accuracy or improved efficiency. These include energy dependent ion transport problems which can exhibit nearly discontinuous solutions[5] since in many cases most of the energy is deposited, as are the ions themselves, in the final few nanometers of the ion range. Another possible application is for multi-dimensional problems where the geometry specifications are complicated and cannot be easily modified or refined. The question remains whether it is possible to implement the *p*-adaptive scheme efficiently in such situations; that is, when and under what circumstances the associated increased computational demands are compensated by the improved numerical properties.

APPENDIX A.

The analytical S_N angular fluxes were computed using a MAPLE implementation of Davison's[37,38] solution for slab geometry. The roots γ_s (M of them, in general, for an $M-$point quadrature set) of the characteristic equation

$$\frac{c}{2}\sum_{1}^{M}\frac{w_m}{1+\mu_m\gamma_s}=1 \tag{26}$$

are used to calculate the coefficients A_s of the angular flux expansions,

$$\psi_m(x)=\frac{c}{2}\sum_{s}\frac{A_s}{1+\mu_m\gamma_s}e^{\sigma_t\gamma_s x}. \tag{27}$$

The coefficients are uniquely determined by boundary conditions at the slab faces and continuity conditions at material interfaces.

Taking into account the special cases of $c=0$ (purely absorbing regions), $\sigma_t=0$ (void regions) and $c=1$ (purely scattering regions), the MAPLE implementation is capable of solving for the fluxes in multi-region slabs

with beam or isotropic incident flux boundary conditions, and vacuum or reflective boundary conditions. Piecewise constant, isotropic distributed sources can also be treated. It is therefore possible to derive expressions for several of the numerical problems investigated. We now give expressions for the scalar flux derived by solving the discrete ordinates equations with an S_8 Lobatto quadrature. The first is given for the heterogeneous slab in Problem 2 and the second is for the homogeneous slabs in Problem 3.

Quadrature data was specified with an accuracy of about 16 digits, and 25 digits of precision in software was used to compute the analytical solutions. We present the result to approximately 15 significant digits. The fluxes are given in units of $\text{cm}^2\ \text{s}^{-1}$. They can be integrated over a cell i from $x_{i-\frac{1}{2}}$ to $x_{i+\frac{1}{2}}$ to obtain an expression for the cell-average scalar flux which may be compared to the transport code solution.

A.1. Scalar Flux for Problem 2

Expressions for the scalar fluxes in each of the regions in Problem 2 follow (refer to Table 2 for material and geometry properties). The boundary condition is reflective on the left face of the slab. Note that there is a void region with a constant flux in the third region of the slab.

Region 1, $0.0 \leq x \leq 2.0$:

$$\begin{aligned}\phi^{\text{exact}}(x) = 1.0 &\\ &- 1.31177193682224 \cdot 10^{-45} \cosh(50.0\,x)\\ &- 3.17415007010824 \cdot 10^{-51} \cosh(57.3565414940264\,x)\\ &- 1.36451484410932 \cdot 10^{-74} \cosh(84.5022556506510\,x)\\ &- 1.30631283781881 \cdot 10^{-208} \cosh(238.892435915824\,x)\end{aligned} \tag{28a}$$

Region 2, $2.0 \leq x \leq 3.0$:

$$\begin{aligned}\phi^{\text{exact}}(x) = 393.329746335834\, e^{-5.0\,x} &\\ &+ 1.01057638902210 \cdot 10^{4}\, e^{-5.73565414940264\,x}\\ &+ 3.72952293942499 \cdot 10^{6}\, e^{-8.45022556506510\,x}\end{aligned}$$

$$
\begin{aligned}
&+ 1.15953512767398 \cdot 10^{20}\, e^{-23.8892435915824\, x} \\
&+ 3.63327979365626 \cdot 10^{-32}\, e^{23.8892435915824\, x} \\
&+ 3.69313137984836 \cdot 10^{-12}\, e^{8.45022556506510\, x} \\
&+ 7.02512054803739 \cdot 10^{-9}\, e^{5.73565414940264\, x} \\
&+ 1.02676349271661 \cdot 10^{-8}\, e^{5.0\, x}
\end{aligned} \tag{28b}
$$

Region 3, $3.0 \leq x \leq 5.0$:

$$
\phi^{\text{exact}}(x) = 1.10478476129567 \tag{28c}
$$

Region 4, $5.0 \leq x \leq 6.0$:

$$
\begin{aligned}
\phi^{\text{exact}}(x) = 10.0 \\
&- 75.3837102021210\, e^{-0.525429430643348\, x} \\
&- 0.198374058668983\, e^{0.525429430643348\, x} \\
&- 5.10151658992129\, e^{-1.02038566141039\, x} \\
&- 249.432632960793\, e^{-1.40739815939178\, x} \\
&- 5.24079514057600 \cdot 10^{-5}\, e^{1.02038566141039\, x} \\
&- 3.44256073529415 \cdot 10^{-5}\, e^{1.40739815939178\, x} \\
&- 1.07174309237792 \cdot 10^{8}\, e^{-3.88193199422286\, x} \\
&- 1.90798226820663 \cdot 10^{-11}\, e^{3.88193199422286\, x}
\end{aligned} \tag{28d}
$$

Region 5, $6.0 \leq x \leq 8.0$:

$$
\begin{aligned}
\phi^{\text{exact}}(x) &= 31.4960454527129\, e^{-0.525429430643348\, x} \\
&+ 5.69192925775592\, e^{-1.02038566141039\, x} \\
&+ 490.785694198117\, e^{-1.40739815939178\, x} \\
&+ 3.13898501490264 \cdot 10^{9}\, e^{-3.88193199422286\, x} \\
&- 0.00311903166569419\, e^{0.525429430643348\, x} \\
&- 4.81843561909690 \cdot 10^{-7}\, e^{1.02038566141039\, x} \\
&- 1.75906698711757 \cdot 10^{-7}\, e^{1.40739815939178\, x} \\
&- 1.6461053547439 \cdot 10^{-15}\, e^{3.88193199422286\, x}
\end{aligned} \tag{28e}
$$

A.2. Scalar Flux for Problem 3

We give two expressions for scalar flux in the 32 cm thick homogeneous slab

with a total cross section of unity and an unnormalized isotropic incident flux on the left face of the slab as in Eq. 7b. The first expression is for the case $c = 0.9$:

$$\begin{aligned}\phi^{\text{exact}}(x) &= 2.66745732840005\, e^{-0.525429430643364\, x} \\ &+ 0.0163367441816152\, e^{-1.02038566141039\, x} \\ &+ 0.119426283671677\, e^{-1.40739815939179\, x} \\ &+ 0.235767350338444\, e^{-3.88193199422285\, x} \\ &- 2.90673596693831 \cdot 10^{-15}\, e^{0.525429430643364\, x} \\ &- 3.10809366588664 \cdot 10^{-24}\, e^{1.02038566141039\, x} \\ &- 1.4850139484062 \cdot 10^{-28}\, e^{1.40739815939179\, x} \\ &- 1.2083059936643 \cdot 10^{-62}\, e^{3.88193199422285\, x}.\end{aligned} \tag{29}$$

The next expression is for the case $c = 0.1$:

$$\begin{aligned}\phi^{\text{exact}}(x) &= 0.0979964004168274\, e^{-0.997814414697098\, x} \\ &+ 0.479543679389974\, e^{-1.13372492599316\, x} \\ &+ 0.684369596638519\, e^{-1.66019779432447\, x} \\ &+ 0.790758401534127\, e^{-4.67894130711627\, x} \\ &- 2.38542312443363 \cdot 10^{-32}\, e^{0.997814414697098\, x} \\ &- 1.60443108179632 \cdot 10^{-33}\, e^{1.13372492599316\, x} \\ &- 1.29792238298439 \cdot 10^{-40}\, e^{1.66019779432447\, x} \\ &- 2.20975509483040 \cdot 10^{-82}\, e^{4.67894130711627\, x}\end{aligned} \tag{30}$$

REFERENCES

1. R. E. Alcouffe, E. W. Larsen, W. F. Miller, and B. R. Wienke, "Computational Efficiency of Numerical Methods for the Multigroup, Discrete Ordinates Neutron Transport Equations: The Slab Geometry Case," *Nucl. Sci. and Engr.*, v. 71, p. 111, 1979.

2. M. L. Adams, "Slab-Geometry Discrete Ordinates Methods," *Trans. of the Am. Nucl. Soc.*, v. 71, p. 217, 1994.

3. K. D. Lathrop, "Spatial Differencing of the Transport Equation: Positivity vs. Accuracy," *J. Comp. Phys.*, v. 4, p. 475, 1969.

4. T. A. Wareing, "An Exponential Discontinuous Scheme for for Discrete-

Ordinate Calculations in Cartesian Geometries," *Proceedings of the Joint International Conference on Mathematical Methods and Supercomputing for Nuclear Applications*, v. 2, p. 1257, 1997.

5. A. K. Prinja and L. J. Lorence, "Exponential Discontinuous Numerical Solutions for Electron Transport in the Continuous Slowing Down Approximation," *Proceedings of the Joint International Conference on Mathematical Methods and Supercomputing for Nuclear Applications*, v. 2, p. 1467, 1997.

6. R. E. Alcouffe, "Diffusion Synthetic Acceleration Methods for Diamond-Differenced Discrete-Ordinates Equations," *Nucl. Sci. and Engr.*, v. 64, p. 344, 1982.

7. E. W. Larsen, "Unconditionally Stable Diffusion-Synthetic Acceleration Methods for Slab Geometry Discrete Ordinates Equations. Part I: Theory," *Nucl. Sci. and Engr.*, v. 82, p. 47, 1982.

8. E. W. Larsen, "Unconditionally Stable Diffusion-Synthetic Acceleration Methods for Slab Geometry Discrete Ordinates Equations. Part II: Numerical Results," *Nucl. Sci. and Engr.*, v. 82, p. 64, 1982.

9. A. M. Voloschenko, "Geometrical Interpretation of Family of Weighted Nodal Schemes and Adaptive Positive Approximations for Transport Equation," *Proceedings of the Joint International Conference on Mathematical Methods and Supercomputing for Nuclear Applications*, v. 2, p. 1517, 1997.

10. T. A. Germogenova, A. V. Shwetsov, and A. M. Voloschenko, "New Difference Schemes for the Neutron Transport Equation," *Trans. Theory and Stat. Phys.*, v. 23, p. 923, 1994.

11. J. P. Hennart, "A Unified Formalism for Spatial Discretization Schemes of Transport Equations in Slab Geometry," *Annals of Nucl. Energy*, v. 8, p. 677, 1981.

12. J. P. Hennart and E. del Valle, "A Generalized Nodal Finite Element Formalism For Discrete Ordinates Equations in Slab Geometry - Part I: Theory in the Continuous Moment Case," *Trans. Theory and Stat. Phys.*, v. 24, p. 449, 1995.

13. J. P. Hennart and E. del Valle, "A Generalized Nodal Finite Element Formalism For Discrete Ordinates Equations in Slab Geometry - Part II: Theory in the Discontinuous Moment Case," *Trans. Theory and Stat. Phys.*, v. 24, p. 479, 1995.

14. J. P. Hennart and E. del Valle, "A Generalized Nodal Finite Element Formalism For Discrete Ordinates Equations in Slab Geometry - Part III: Numerical Results," *Trans. Theory and Stat. Phys.*, v. 24, p. 505, 1995.

15. W. F. Walters and T. A. Wareing, "An Accurate, Strictly-Positive, Non-Linear Characteristic Scheme for the Discrete-Ordinate Equations," *Trans. Theory and Stat. Phys.*, v. 25, p. 197, 1996.

16. R. T. Ackroyd, et al., **Some Recent Development in Finite Element Methods for Neutron Transport** in *Advances in Nuclear Science and Technology* (J. Lewins and M. Becker, eds.), Vol. 19, New York: Plenum Press, 1987.

17. R. T. Ackroyd, "Generalized Least-Squares as a Generator of Variational Principles and Weighted-Residual Methods for FEM Transport," *Prog. in Nucl. Energy*, v. 18, p. 45, 1986.

18. T. R. Hill, "ONETRAN: A Discrete Ordinates Finite Element Code for the Solution of the One-Dimensional Multigroup Transport Equation," LA-5990-MS, Los Alamos National Laboratory, Jun 1975.

19. H. G. Kaper, G. K. Leaf, and A. J. Lindeman, "Applications of Finite Element Methods in Reactor Mathematics: Numerical Solution of the Neutron Transport Equation," ANL-8126, Argonne National Laboratory, Oct 1974.

20. W. R. Martin, C. E. Yehnert, L. Lorence, and J. J. Duderstadt, "Phase-Space Finite Element Methods Applied to the First-Order Form of the Transport Equation," *Annals of Nucl. Energy*, v. 8, p. 633, 1981.

21. W. R. Martin and J. J. Duderstadt, "Finite Element Solutions of the Neutron Transport Equation with Applications to Strong Heterogeneities," *Nucl. Sci. and Engr.*, v. 62, p. 371, 1977.

22. J. E. Morel, J. E. Dendy, and T. A. Wareing, "Diffusion-Accelerated Solution of the Two-Dimensional S_n Equations with Bilinear-Discontinuous Differencing," *Nucl. Sci. and Engr.*, v. 115, p. 304, 1993.

23. M. L. Adams and W. R. Martin, "Diffusion Synthetic Acceleration of Discontinuous Finite Element Transport Iterations," *Nucl. Sci. and Engr.*, v. 111, p. 145, 1992.

24. J. S. Warsa, **Time Dependent Numerical Transport with Application to Thin Slabs**. Master's Thesis, University of New Mexico, Dec 1993.

25. Y. Y. Azmy, "The Weighted Diamond-Difference Form of Nodal Transport Methods," *Nucl. Sci. and Engr.*, v. 98, p. 29, 1988.

26. B. W. Char, et al., **Maple Reference Manual.** Waterloo, Ontario: Waterloo Maple Software, 1988.

27. R. A. Shapiro, **Adaptive Finite Element Solution for the Euler Equations** in *Notes on Num. Fluid Mech.*, Vol. 32, Braunschweig: Vieweg, 1991.

28. R. Biswas, K. D. Devine, and J. E. Flaherty, "Parallel, Adaptive Finite Element Methods for Conservation Laws," *Appl. Num. Math.*, v. 14, p. 255, 1994.

29. O. C. Zienkiewicz and R. L. Taylor, **The Finite Element Method, Volume 1.** London: McGraw-Hill, Fourth Ed., 1989.

30. I. Babuska, M. Griebel, and J. Pitkaranta, "The Problem of Selecting the Shape Functions for a *p*-Type Finite Element," *Int. J. for Num. Meth. Engr.*, v. 28, p. 1891, 1989.

31. D. C. Carpenter, "Two-Dimensional Finite Element Neutron Diffusion Analysis Using Hierarchic Shape Functions," *Proceedings of the Joint International Conference on Mathematical Methods and Supercomputing for Nuclear Applications*, v. 1, p. 603, 1997.

32. M. S. Lazo and J. E. Morel, "A Linear Discontinuous Galerkin Approximation for the Continuous Slowing Down Operator," *Nucl. Sci. and Engr.*, v. 92, p. 98, 1986.

33. E. W. Larsen and P. Nelson, "Finite-Difference Approximations and Superconvergence for the Discrete-Ordinates Equations in Slab Geometry," *SIAM J. Numer. Anal.*, v. 19, p. 334, 1982.

34. E. W. Larsen and W. F. Miller, "Convergence Rates of Spatial Difference Equations for the Discrete-Ordinates Neutron Transport Equations in Slab Geometry," *Nucl. Sci. and Engr.*, v. 73, p. 76, 1980.

35. R. H. Szilard and G. C. Pomraning, "A Modified Linear Discontinuous Spatial Discretization Method in Planar Geometry," *Trans. Theory and Stat. Phys.*, v. 18, p. 255, 1989.

36. W. H. Reed, "New Difference Schemes for the Neutron Transport Equation," *Nucl. Sci. and Engr.*, v. 46, p. 309, 1971.

37. K. Mathews, G. Sjoden, and B. Minor, "Exponential Characteristic Spa-

tial Quadrature for Discrete Ordinates Radiation Transport in Slab Geometry," *Nucl. Sci. and Engr.*, v. 118, p. 24, 1994.

38. B. Davison, **Neutron Transport Theory**. Oxford, England: Clarendon Press, 1957.

39. J. E. Morel, "A Synthetic Acceleration Method for Discrete Ordinates Calculations with Highly Anisotropic Scattering," *Nucl. Sci. and Engr.*, v. 82, p. 34, 1982.

Received: *18 May 1998*
Accepted: *06 January 1999*